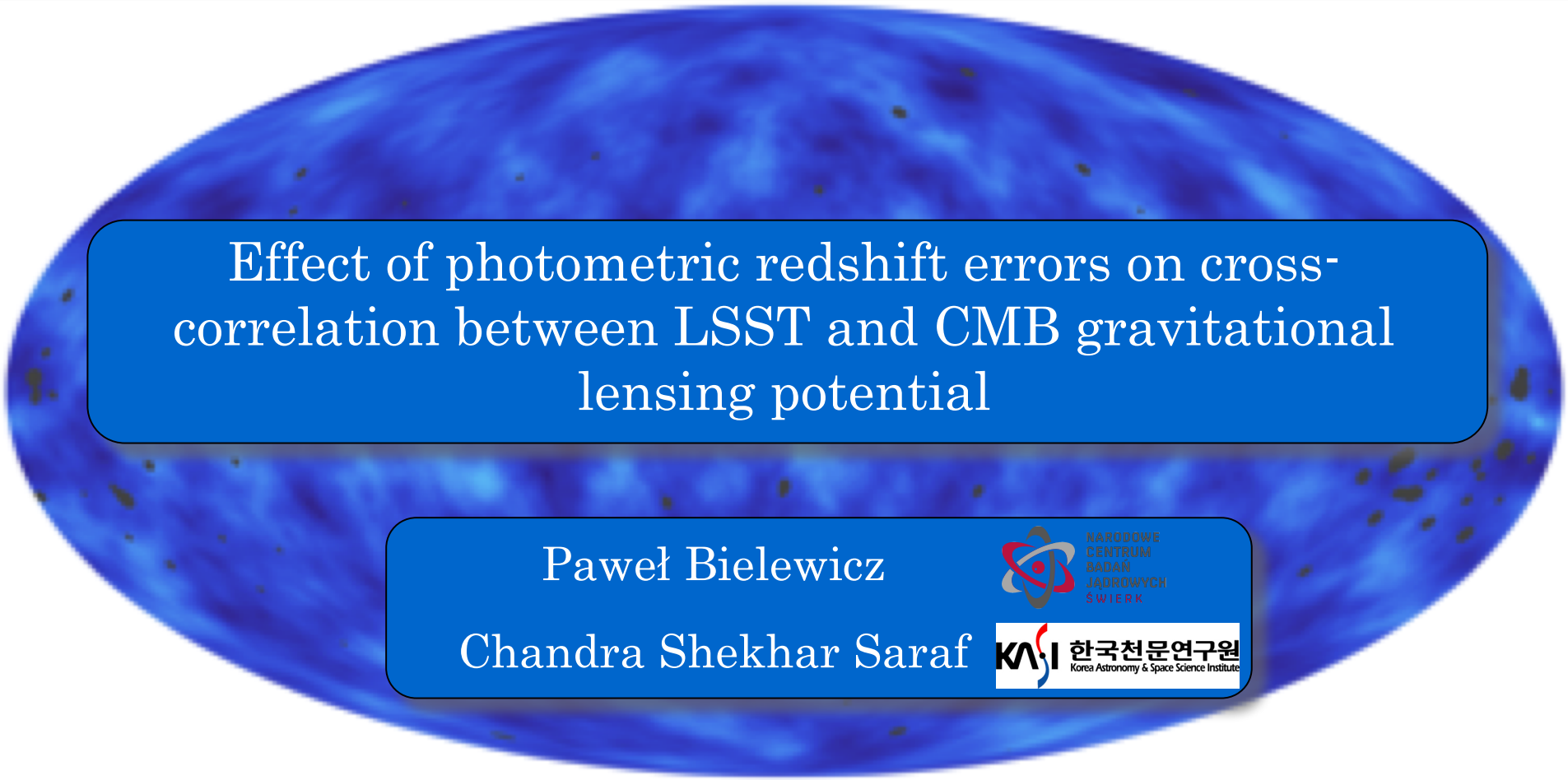

Effect of photometric redshift errors on cross-correlation between LSST and CMB gravitational lensing potential

Paweł Bielewicz

Chandra Shekhar Saraf

NARODOWE CENTRUM BADAŃ JĄDROWYCH ŚWIERK

KASI 한국천문연구원 Korea Astronomy & Space Science Institute

CMB gravitational lensing

- Deflection of the CMB photon paths by the large-scale structure of the Universe (~ 3')
- Correlation of deflection angles over the sky by an angle ~ 2^{o}
- Reconstruction of lensing potential from changes in CMB anisotropy
- Lensing potential as a tracer of dark matter distribution

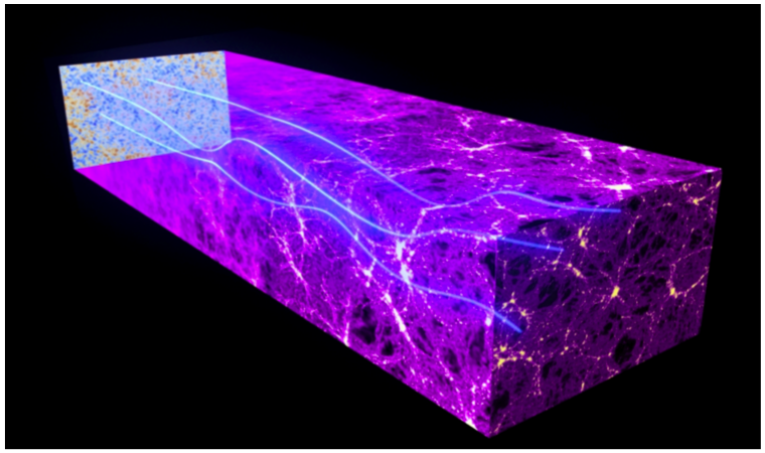

$$\phi(\hat{n}) = -\frac{2}{c^2}\int_0^{\chi_{rec}} d\chi \frac{D_{ls}}{D_l D_s}\Psi(\chi_0 - \chi, \chi\hat{n})$$

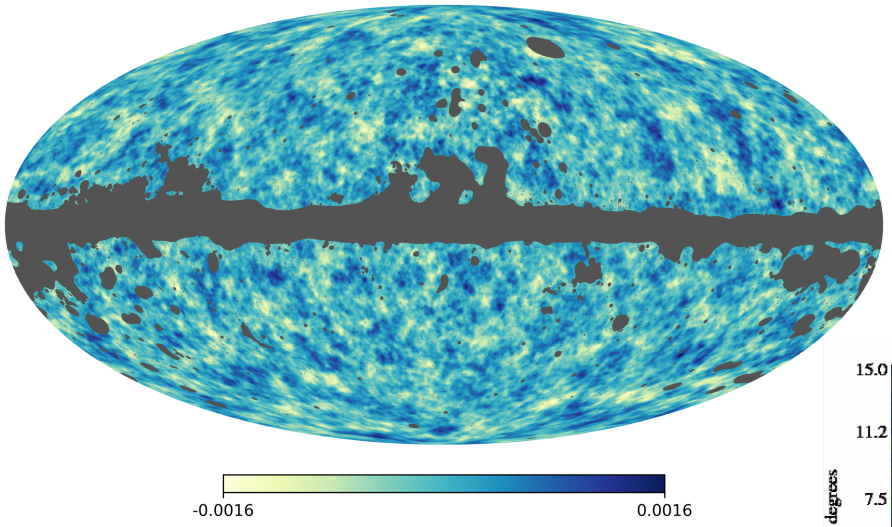

Planck collaboration et al. (2020)

$$\Delta\widetilde{T}(\hat{n}) = \Delta T(\hat{n} + \nabla\phi(\hat{n}))$$

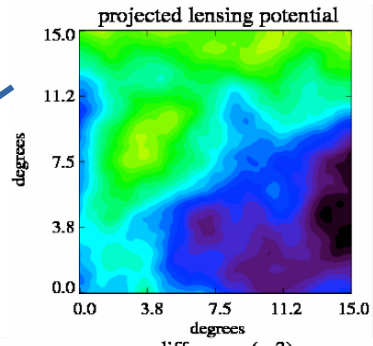

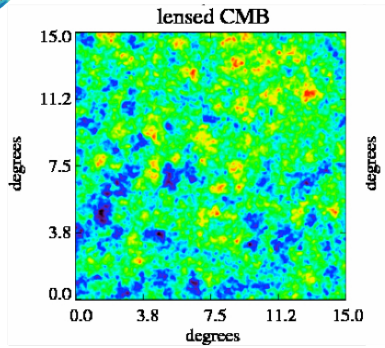

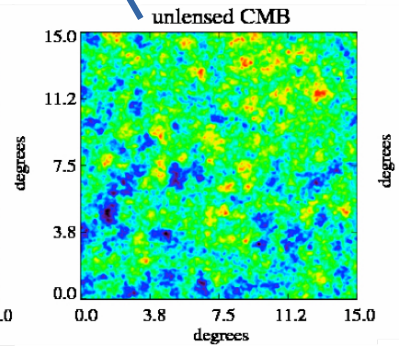

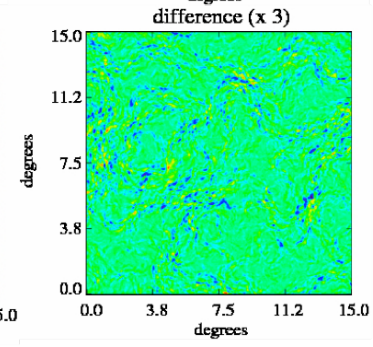

Cross-correlation between CMB lensing and galaxy surveys

- Broad CMB lensing kernel does not allow tracing time evolution of dark matter clustering
- Needed cross-correlation of CMB lensing map with objects with known redshift (galaxies, quasars, radio sources, etc.)
- Splitting redshift distribution on redshift bins (cosmic tomography: White et al. 2022; Pandey et al. 2022; Chang et al. 2022; Sun et al. 2022; Krolewski et al. 2021; Hang et al. 2021; Peacock & Bilicki 2018, Saraf et al. 2024)

$$\phi(\hat{n}) = -\frac{2}{c^2}\int_0^{\chi_{rec}} d\chi \frac{D_{ls}}{D_l D_s}\Psi(\chi_0 - \chi, \chi\hat{n})$$

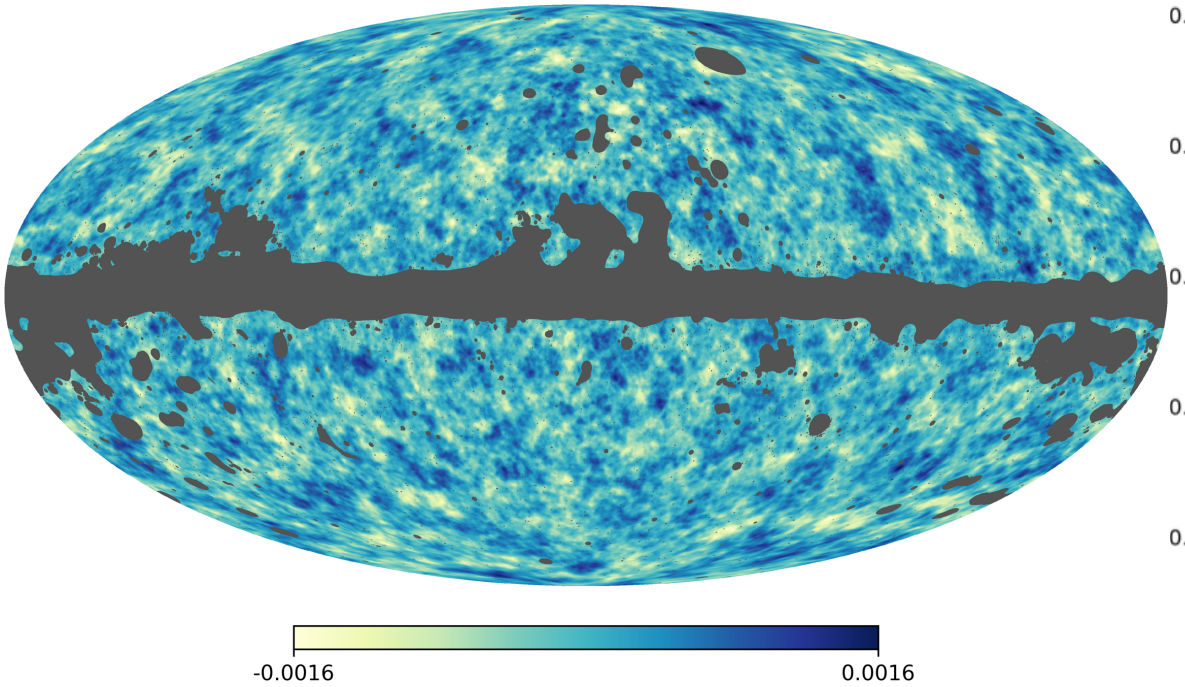

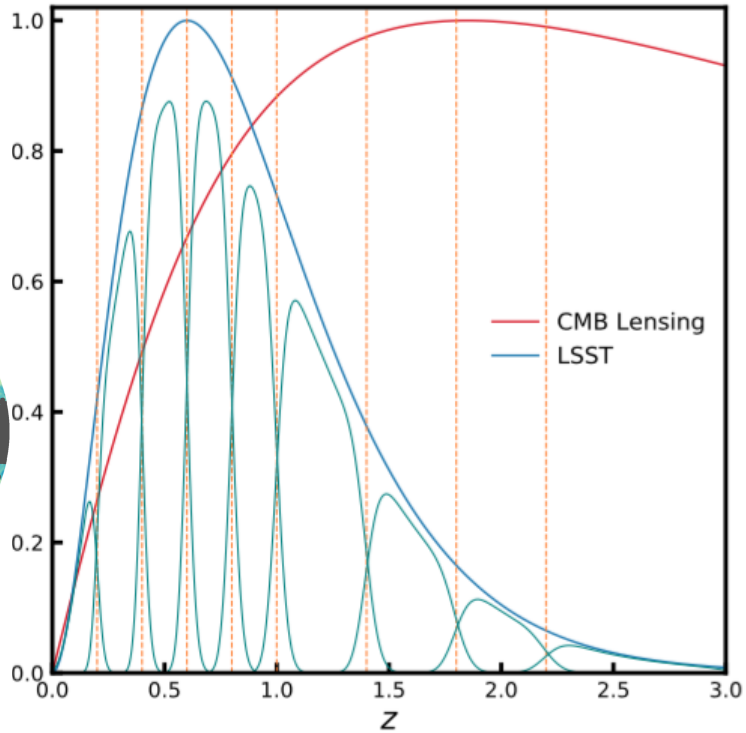

Saraf, PB (2024)

Cross-correlation power spectrum

- Estimation of σ_8 and galaxy bias parameters from the angular power spectra of the lensing potential and galaxy distribution
- Cross-power spectrum between CMB lensing and galaxy density contrast

$$C_\ell^{\kappa g} = \int_0^{\chi_*} \mathrm{d}\chi \frac{W^\kappa(\chi)\, W^g(\chi)}{\chi^2} P_m\left(k = \frac{\ell + 1/2}{\chi}, z(\chi)\right) \qquad \theta \sim \frac{\pi}{\ell}$$

$$\kappa(\hat{\mathbf{n}}) = -\frac{1}{2}\nabla^2\phi(\hat{\mathbf{n}})$$

$$g = \frac{n - \bar{n}}{\bar{n}}$$

$$W^\kappa(\chi) = \frac{3\,\Omega_m}{2\,c^2} H_0^2 (1+z)\,\chi\,\frac{\chi_* - \chi}{\chi_*}$$

$$\mathrm{W}^g(\chi) = b(z(\chi))\,\frac{H(\chi)}{c}\,\frac{\mathrm{d}N}{\mathrm{d}z(\chi)}$$

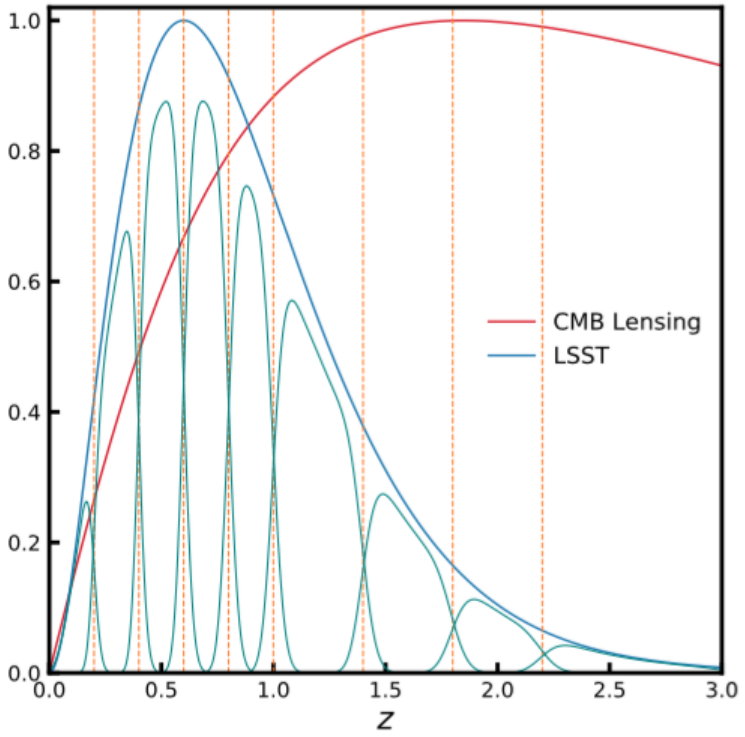

Testing tomographic cross-correlation

- Test using simulations of LSST galaxy survey
- 300 simulations of correlated log-normal galaxy over-density (with LSST Science Book redshift distribution) and CMB lensing convergence fields (consistent with Planck CMB lensing map) using Full-sky Lognormal Astro-fields Simulation Kit (FLASK) code (Xavier et al. 2016)

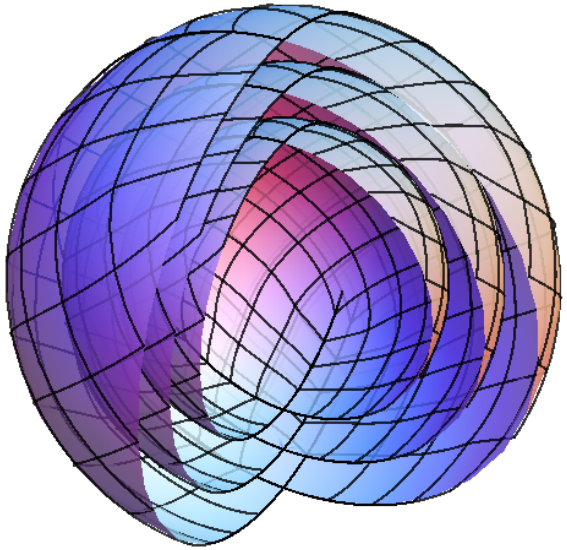

Tomographic binning of redshift distribution

- Photometric redshifts z_p obtained by adding Gaussian or Lorentzian photo-z errors to true redshifts z_t

$$\frac{dN(z_p)}{dz_p} = \int dz_t \frac{dN(z_t)}{dz_t} p(z_p - z_t|z_t)$$

$$p(z_p - z_t|z_t) = \mathcal{G}(z_t, \sigma(z_t))$$

$$\sigma(z) = \sigma_0(1+z)$$

$$p(z_p - z_t|z_t) \propto \left[1 + \frac{1}{2a}\left(\frac{z_p - z_t}{\gamma_0(1+z_t)}\right)^2\right]^{-a}$$

$\sigma_0 = 0.02$

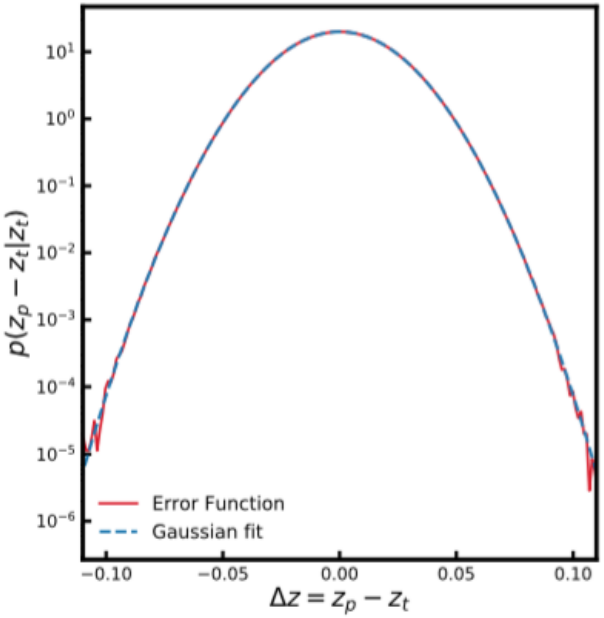

$\sigma_0 = 0.05$

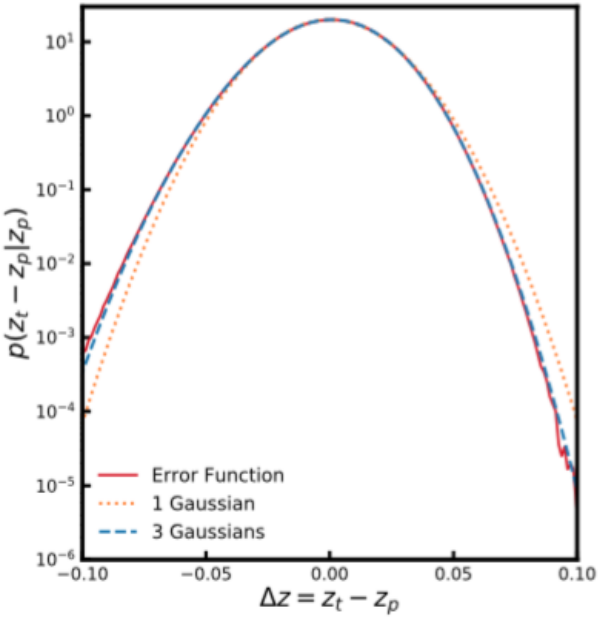

$\gamma_0 = 0.02$

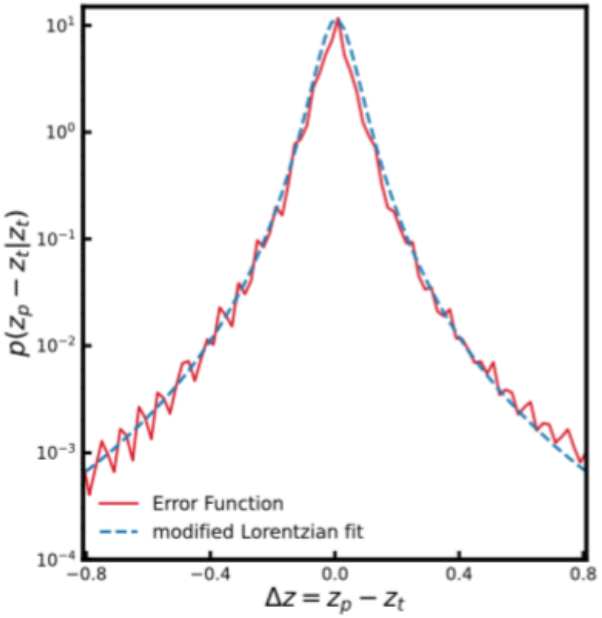

Saraf, PB (2024)

Tomographic binning of redshift distribution

- Photometric redshifts z_p obtained by adding Gaussian or Lorentzian photo-z errors to true redshifts z_t

$$\frac{dN(z_p)}{dz_p} = \int dz_t \frac{dN(z_t)}{dz_t} p(z_p - z_t|z_t)$$

- Tomographic binning of the true redshift distribution

$$\frac{dN^i(z_p)}{dz_p} = \int dz_t \frac{dN(z_t)}{dz_t} W^i(z_t) p^i(z_p - z_t|z_t) \qquad W^i(z_t) = \begin{cases} 1, & \text{if } z^i_{\min} \le z_t < z^{i+1}_{\min} \\ 0, & \text{otherwise} \end{cases}$$

$\sigma_0 = 0.02$ $\sigma_0 = 0.05$ $\gamma_0 = 0.02$

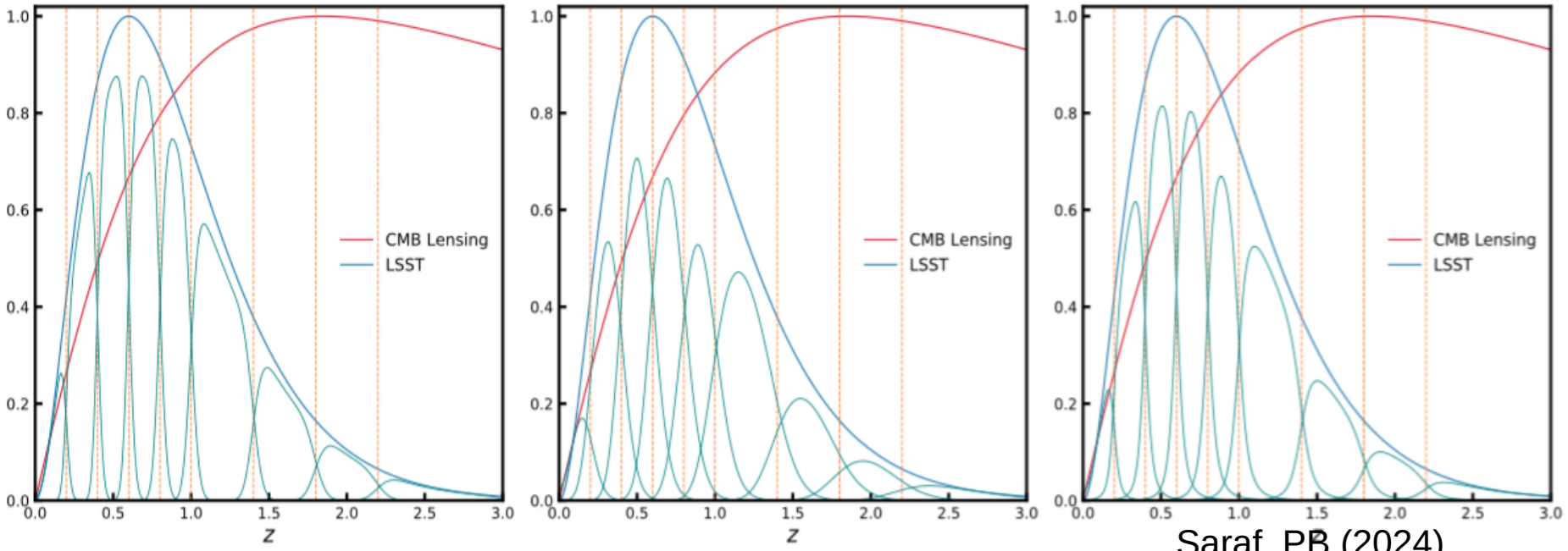

Saraf, PB (2024)

Tomographic binning of redshift distribution

- Photometric redshifts z_p obtained by adding Gaussian or Lorentzian photo-z errors to true redshifts z_t

$$\frac{dN(z_p)}{dz_p} = \int dz_t \frac{dN(z_t)}{dz_t} p(z_p - z_t|z_t)$$

- Tomographic binning of the true redshift distribution

$$\frac{dN^i(z_p)}{dz_p} = \int dz_t \frac{dN(z_t)}{dz_t} W^i(z_t) p^i(z_p - z_t|z_t) \qquad W^i(z_t) = \begin{cases} 1, & \text{if } z^i_{\min} \le z_t < z^{i+1}_{\min} \\ 0, & \text{otherwise} \end{cases}$$

- Simple model of power spectra for galaxies with photo-z

$$C_i^{gg,ph}(\ell) = \int_0^{\chi_*} \frac{d\chi}{\chi^2} \left(b(z_p) \frac{dN^i(z_p)}{dz_p} \right)^2 P_m \left(k = \frac{\ell + 1/2}{\chi}, z_p(\chi) \right)$$

$$C_i^{\kappa g,ph}(\ell) = \int_0^{\chi_*} \frac{d\chi}{\chi^2} W^\kappa(\chi)\, b(z_p) \frac{dN^i(z_p)}{dz_p} P_m \left(k = \frac{\ell + 1/2}{\chi}, z_p(\chi) \right)$$

Power spectra for tomographic analysis

- Power spectra for galaxies with photometric redshifts are related to power spectra for galaxies with true redshifts by (Zhang et al. 2010):

$$C_{ij}^{gg,ph}(\ell) = \sum_k P_{ki}\, P_{kj}\, C_{kk}^{gg,tr}(\ell)$$

$$C_{i}^{\kappa g,ph}(\ell) = \sum_k P_{ki}\, C_{kk}^{\kappa g,tr}(\ell)$$

where $P_{ij} \equiv \dfrac{N_{i\to j}}{N_j^{ph}}$ is so called scattering matrix ($\sum_i P_{ij} = 1$)

$$C_{kk}^{gg,tr}(\ell) = \int_0^{z_*} \frac{\mathrm{d}z_t}{c} \frac{H(z_t)}{\chi^2(z_t)} \left(b(z_t) \frac{dN(z_t)}{dz_t} \right)^2 W^k(z_t)\, P_m\left(k = \frac{\ell + 1/2}{\chi(z_t)}, z_t\right)$$

$$C_{kk}^{\kappa g,tr}(\ell) = \int_0^{z_*} \frac{\mathrm{d}z_t}{c} \frac{H(z_t)}{\chi^2(z_t)} W^{\kappa}(z_t)\, b(z_t) \frac{dN(z_t)}{dz_t} W^k(z_t)\, P_m\left(k = \frac{\ell + 1/2}{\chi(z_t)}, z_t\right)$$

Power spectra for tomographic analysis

- Power spectra for galaxies with photometric redshifts are related to power spectra for galaxies with true redshifts by (Zhang et al. 2010):

$$C_{ij}^{gg,ph}(\ell) = \sum_k P_{ki}\, P_{kj}\, C_{kk}^{gg,tr}(\ell)$$

$$C_{i}^{\kappa g,ph}(\ell) = \sum_k P_{ki}\, C_{kk}^{\kappa g,tr}(\ell)$$

where $P_{ij} \equiv \dfrac{N_{i\to j}}{N_j^{ph}}$ is so called scattering matrix ($\sum_i P_{ij} = 1$)

- Zhang et al. (2017) proposed algorithm, Non-negative Matrix Factorization, to solve for P_{ij} and $C_{kk}^{tr}(\ell)$ having $C_{ij}^{ph}(\ell)$

- With estimation of the true redshift distribution it is possible fast method of computation of the scattering matrix

$\sigma_0 = 0.02$ $\sigma_0 = 0.05$ $\gamma_0 = 0.02$

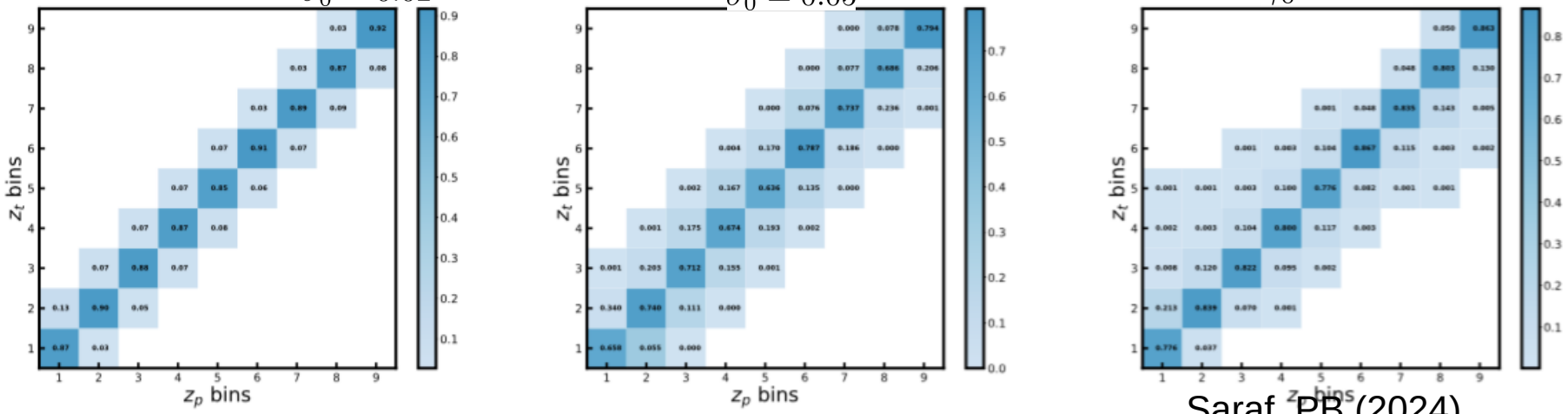

Saraf, PB (2024)

Tests for simulations without correction for photo-z errors

- Estimation of the angular power spectra

$$\hat{C}_L^{xy} = \sum_{L'} K^{-1}_{LL'} \left(\tilde{C}^{xy}_{L'} - \left\langle \tilde{N}^{xy}_{L'} \right\rangle_{MC} \right) \qquad \tilde{C}^{xy}_{\ell} = \frac{\sum_m \tilde{a}^x_{\ell m} \tilde{a}^{y*}_{\ell m}}{2\ell + 1}$$

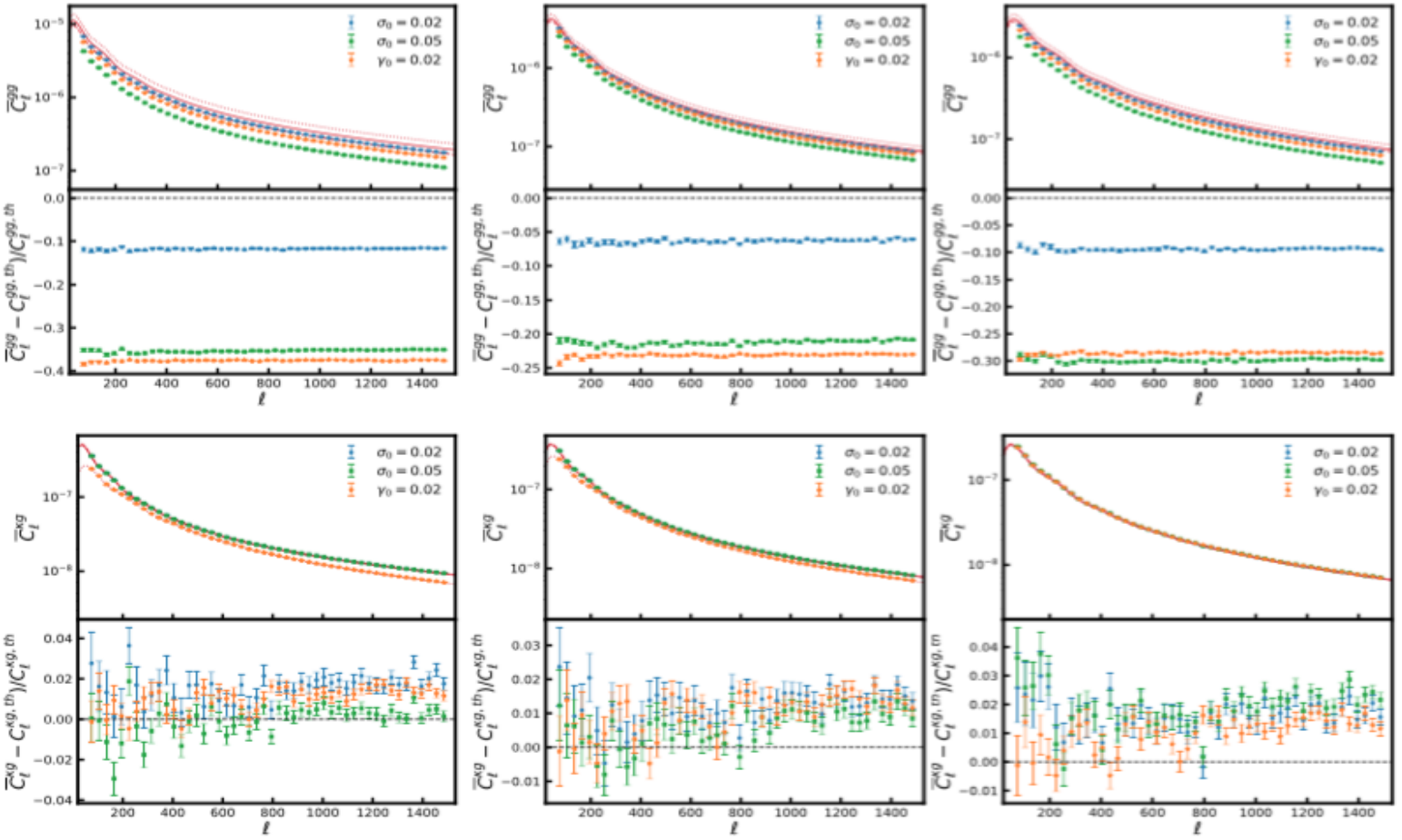

Bin 5 ($0.8 \leq z < 1.0$) Bin 6 ($1.0 \leq z < 1.4$) Bin 7 ($1.4 \leq z < 1.8$)

Saraf, PB (2024)

Tests for simulations after correction for photo-z errors

- Estimation of the angular power spectra

$$\hat{C}_L^{xy} = \sum_{L'} K^{-1}_{LL'} \left(\tilde{C}^{xy}_{L'} - \left\langle \tilde{N}^{xy}_{L'} \right\rangle_{MC} \right) \qquad \tilde{C}^{xy}_{\ell} = \frac{\sum_m \tilde{a}^x_{\ell m} \tilde{a}^{y*}_{\ell m}}{2\ell + 1}$$

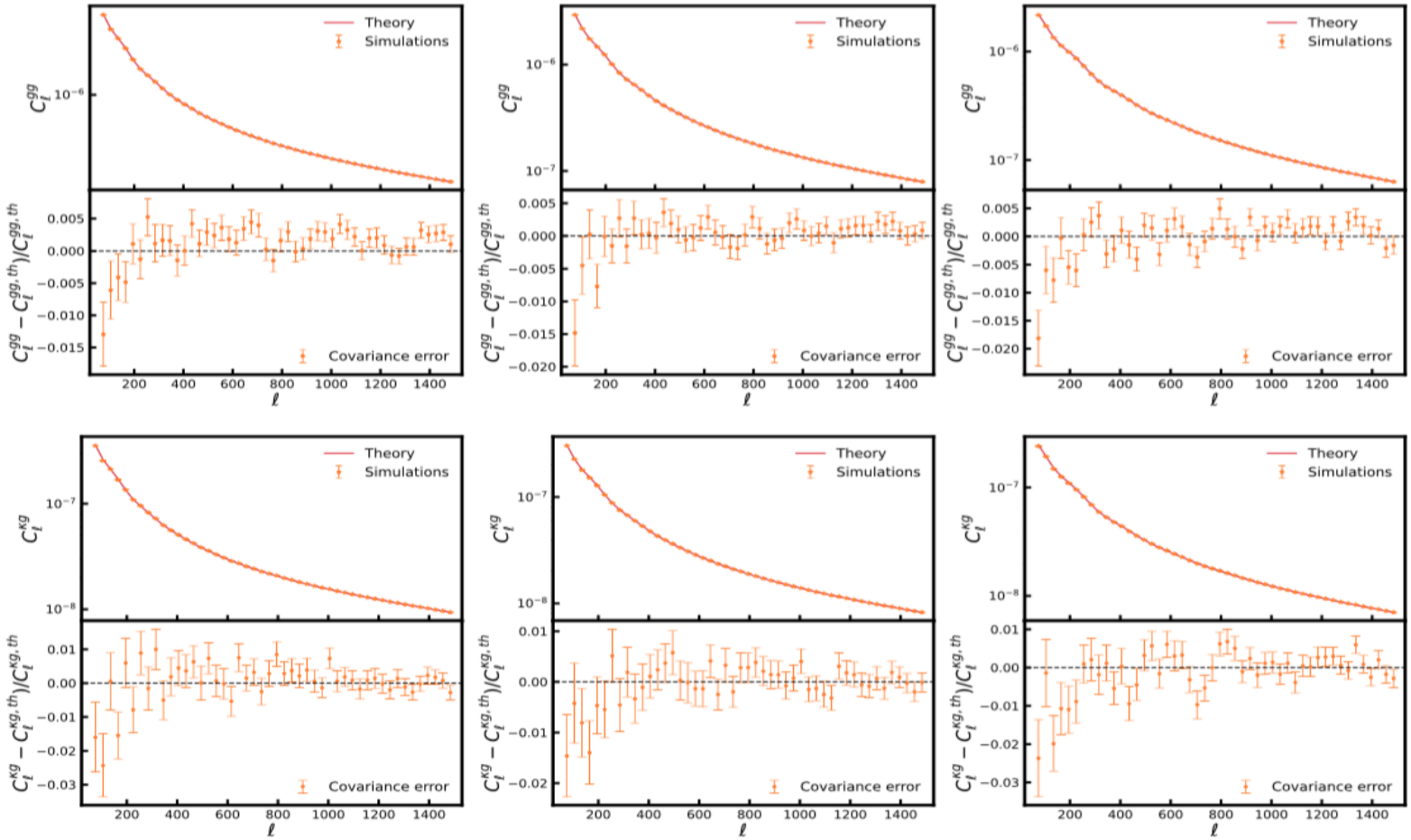

Saraf, PB (2024)

Estimation of the parameters

$$C_L^{gg} \propto b(\bar{z})^2\, C_L^{gg,\mathrm{fid}} \qquad C_L^{\kappa g} \propto A\, b(\bar{z})\, C_L^{\kappa g,\mathrm{fid}}$$

$\sigma_0 = 0.02$ | $\sigma_0 = 0.05$ | $\gamma_0 = 0.02$

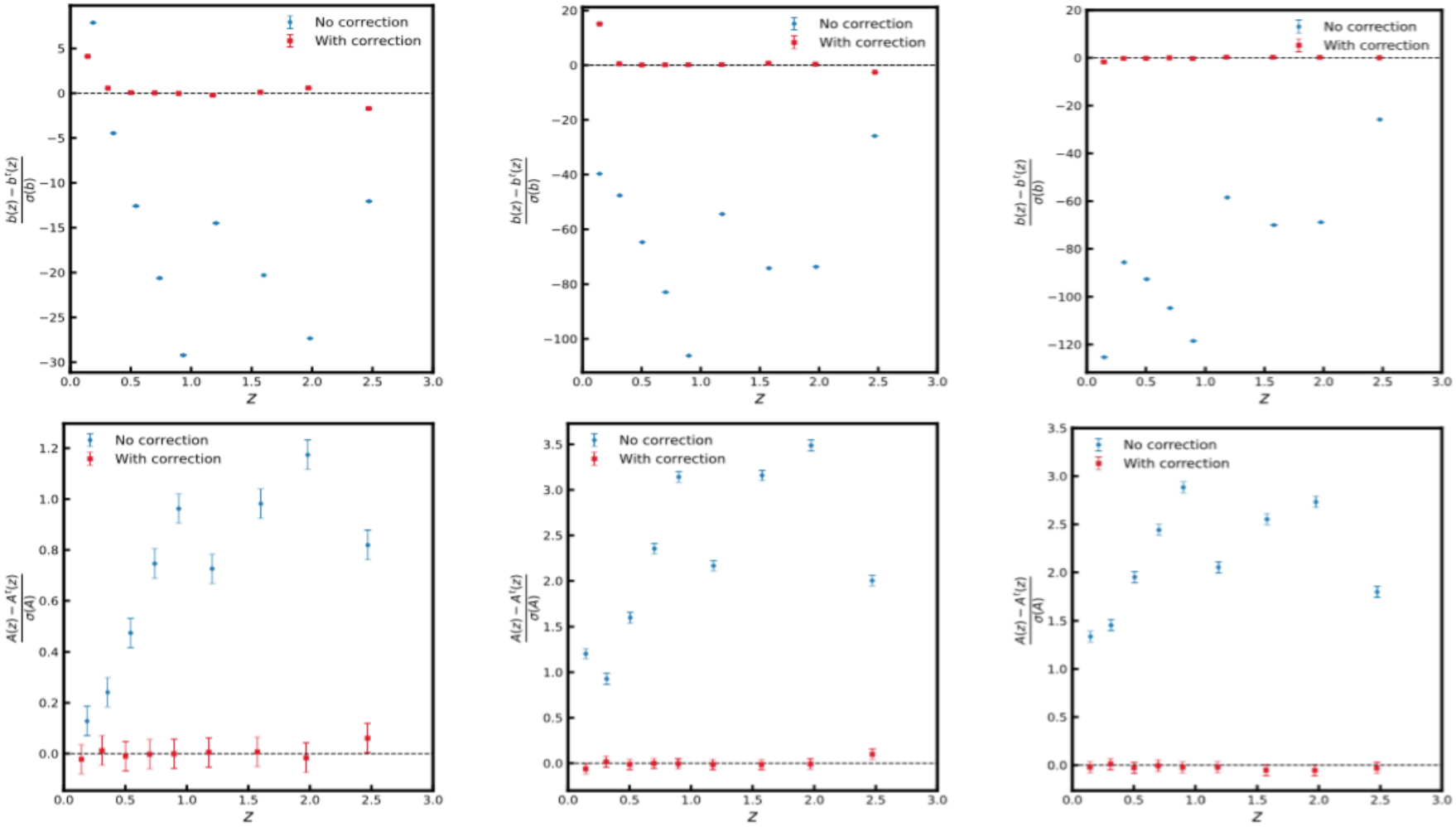

Saraf, PB (2024)

Estimation of the parameters

$$\sigma_8(z) = A(z)\sigma_{8,0}D(z)$$

$\sigma_0 = 0.02$

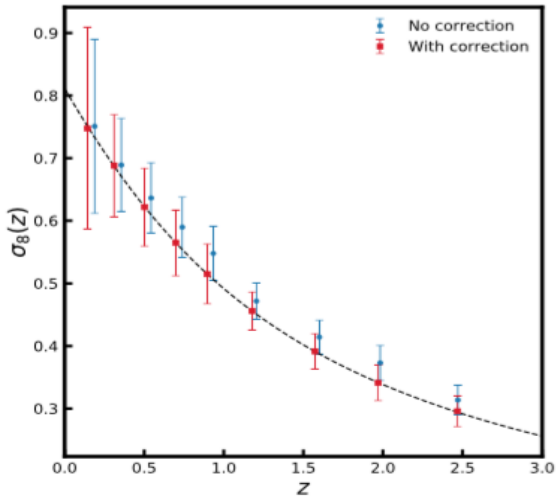

$\sigma_0 = 0.05$

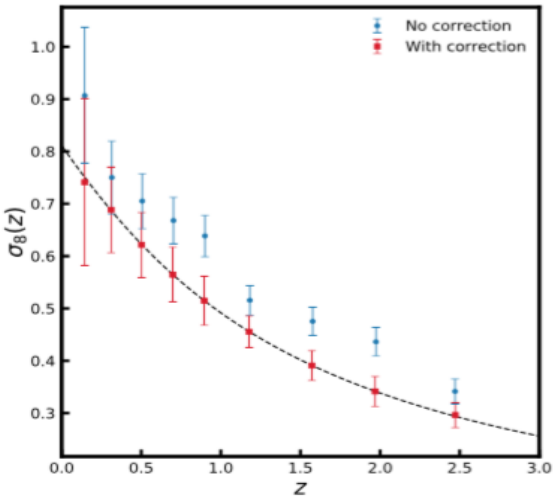

$\gamma_0 = 0.02$

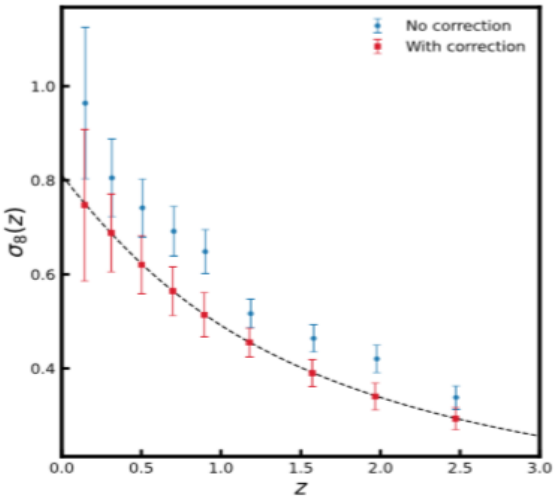

Saraf, PB (2024)

LSST simulations

- Redshift Assessment Infratructure Layers (RAIL)
- Redshifts and six band magnitudes from Buzzard simulations (DeRose et al. 2019)
- Added errors on photometric magnitudes consistent with LSST Y1
- Photo-z estimated using FlexZBoost
- Added correlations with CMB using GLASS (Tessore et al. 2023)

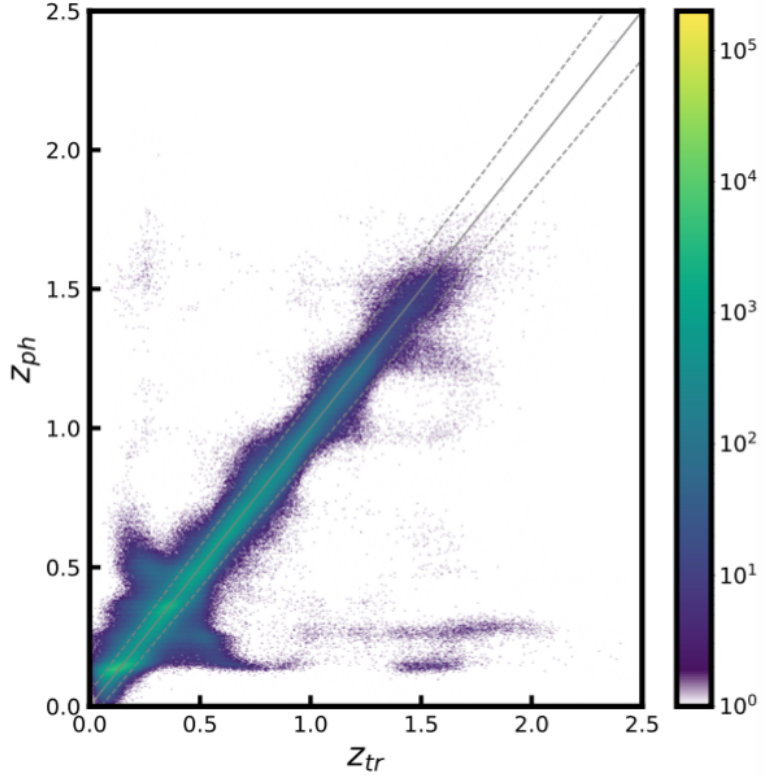

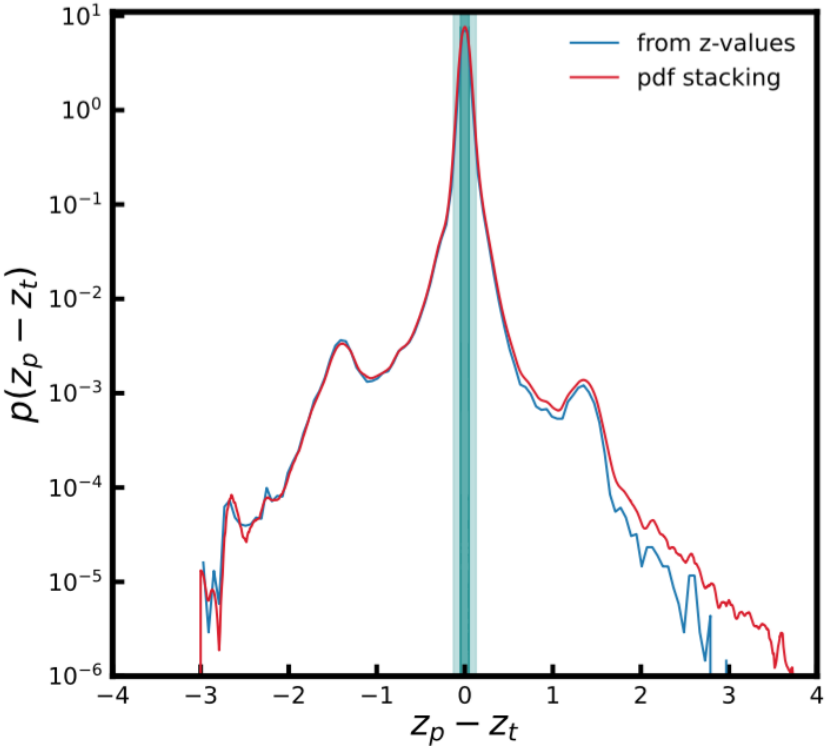

Credit: Ch. Saraf

LSST simulations

- Redshift Assessment Infratructure Layers (RAIL)
- Redshifts and six band magnitudes from Buzzard simulations (DeRose et al. 2019)
- Added errors on photometric magnitudes consistent with LSST Y1
- Photo-z estimated using FlexZBoost
- Added correlations with CMB using GLASS (Tessore et al. 2023)

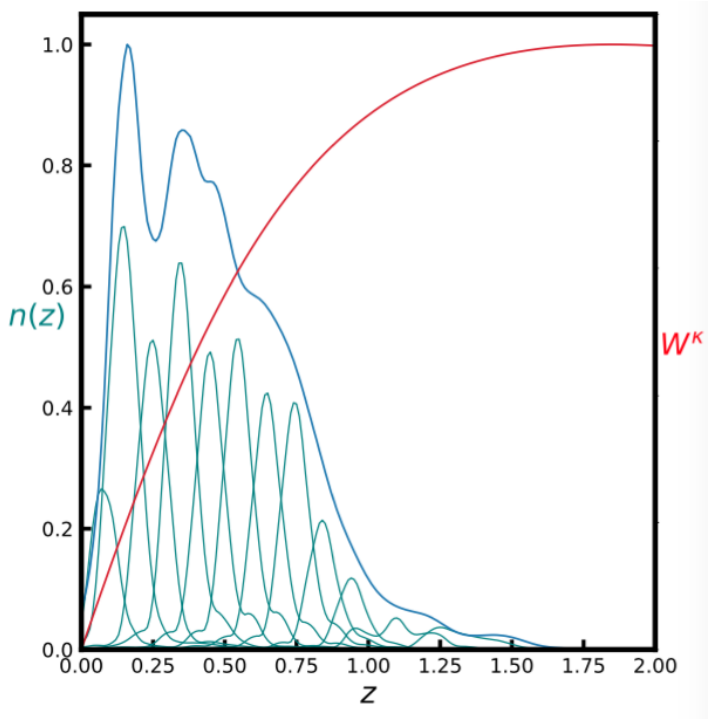

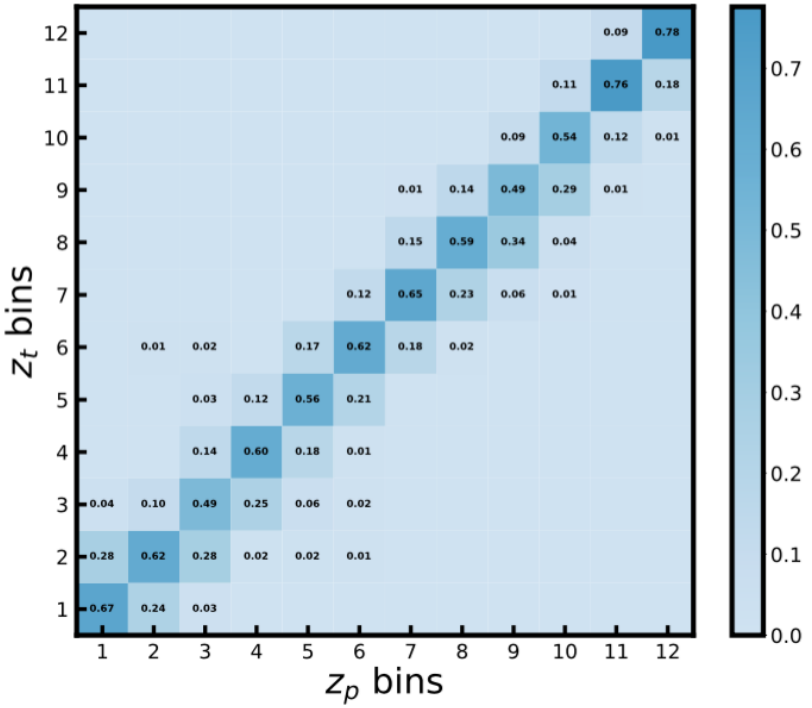

Credit: Ch. Saraf

LSST simulations

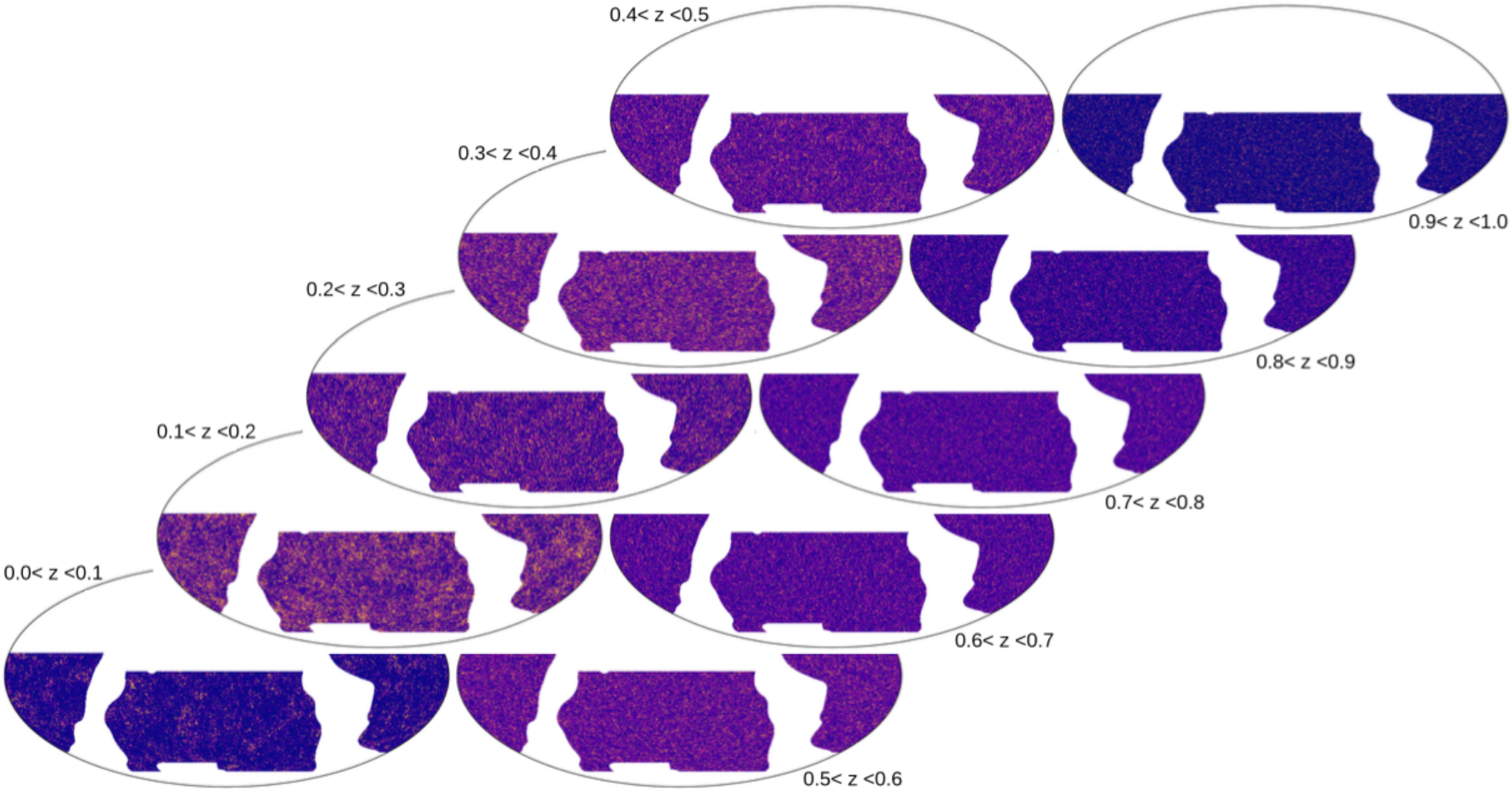

Credit: Ch. Saraf

Estimation of parameters

$S_8 = 0.832 \pm 0.013$ (fiducial)

$S_8 = 0.792 \pm 0.013$ (wout corr)

$S_8 = 0.823 \pm 0.016$ (with corr)

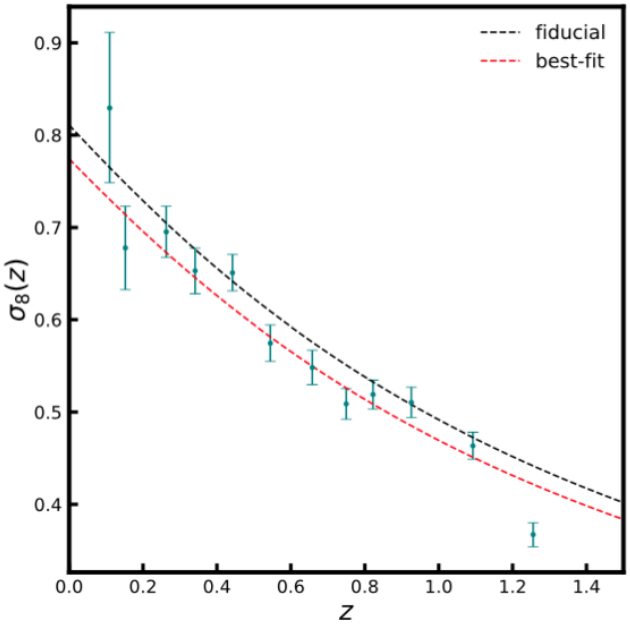

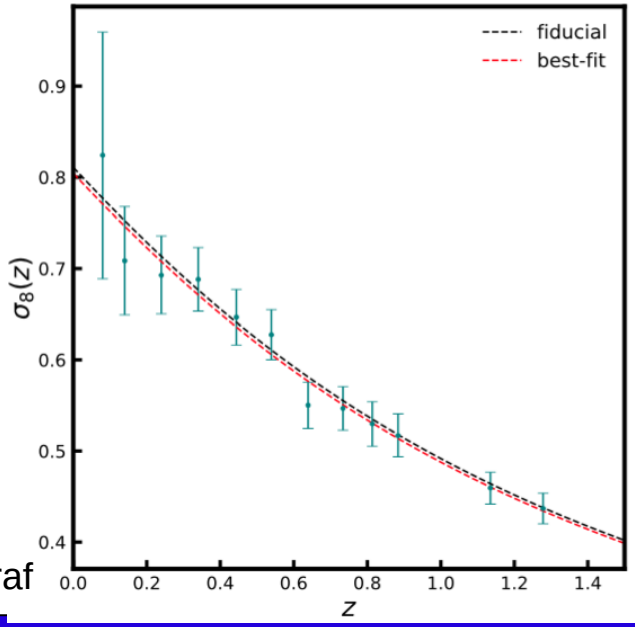

Credit: Ch. Saraf

Correlation with DESI Legacy Imaging Survey

- Cross-correlation between Planck CMB lensing potential and DESI Legacy Imaging Survey (DESI-LIS)

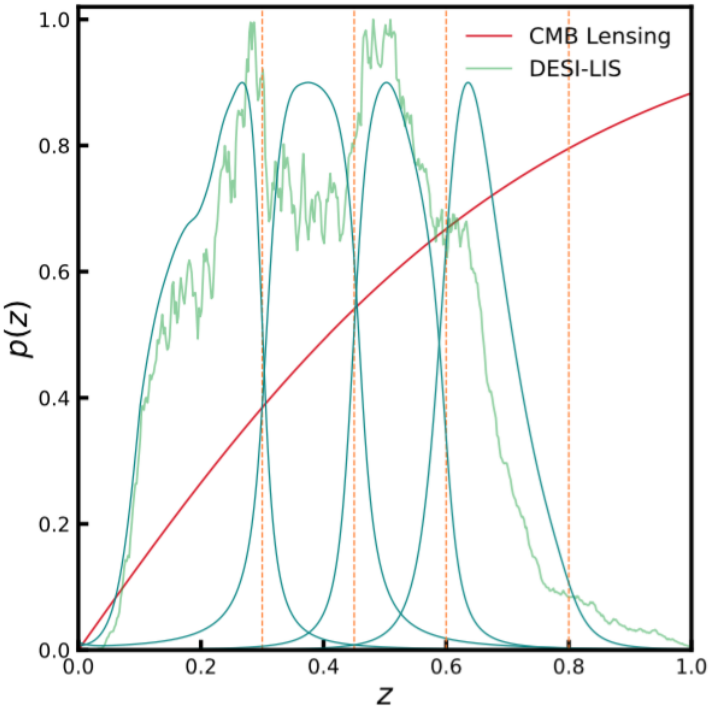

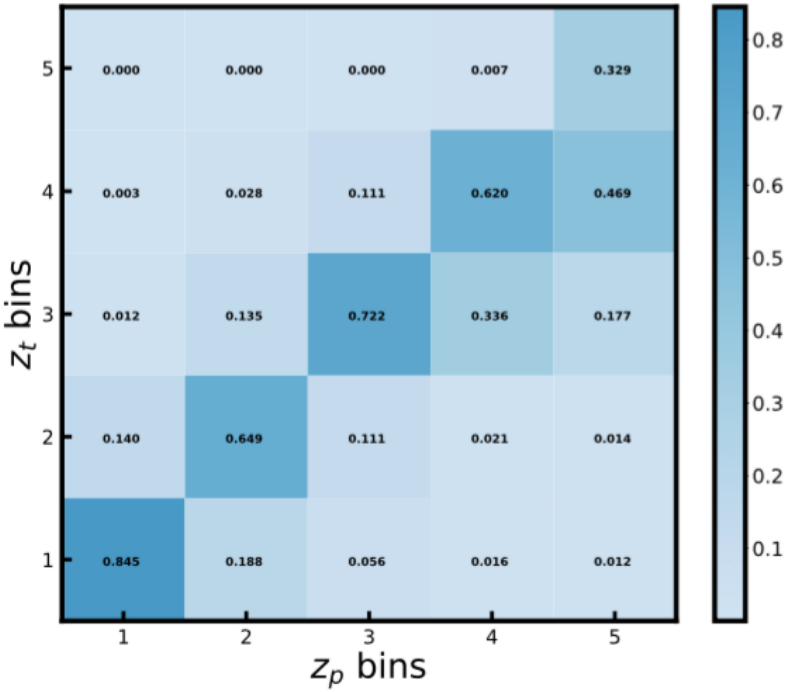

Saraf et al. (2024)

Correlation with DESI Legacy Imaging Survey

- Cross-correlation between Planck CMB lensing potential and DESI Legacy Imaging Survey (DESI-LIS)
- the clustering amplitude more consistent with the ΛCDM model after correction for the redshift bin mismatch (though deviation still present for the first two bins)

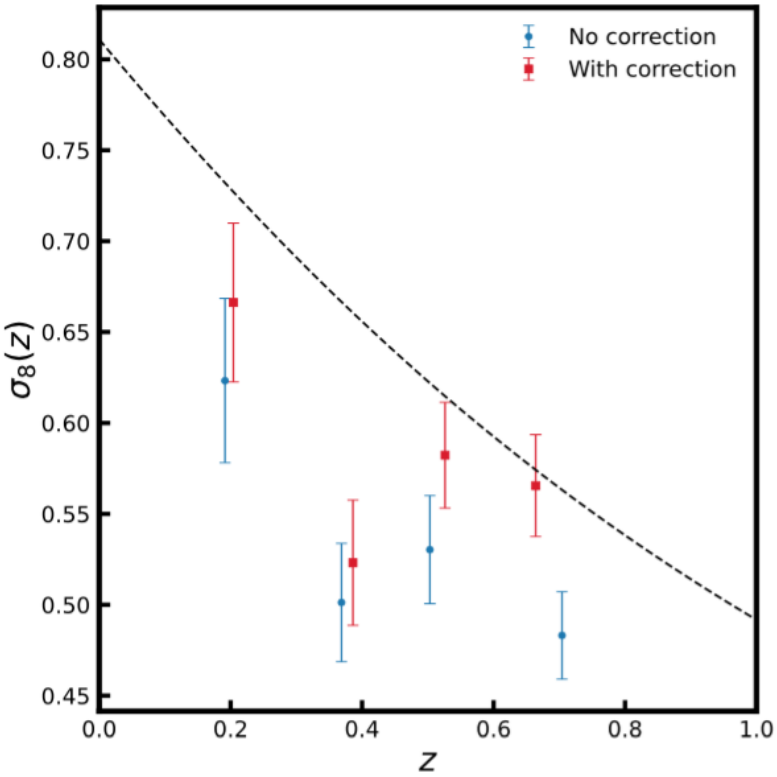

Saraf et al. (2024)

Conclusions

- Tomographic cross-correlation between CMB lensing map and LSST galaxy survey useful for tracing time evolution of the large-scale structure
- Systematic errors caused by redshift bin mismatch of galaxies with photo-z
- ~3σ deviation on S_8 parameter due to bin mismatch for LSST Y1 simulations
- Needed correction for the redshift bin mismatch using scattering matrix formalism
- Potential solution to the S_8 tension in cosmology ?